Environmental Science Nano

Abiotic photomineralization and transformation of iron oxide nanominerals in aqueous systems

Journal:	*Environmental Science: Nano*
Manuscript ID	EN-ART-12-2017-001242.R1
Article Type:	Paper
Date Submitted by the Author:	16-Mar-2018

Complete List of Authors:	Liu, Lihu; Huazhong Agricultural University, College of Resources & Environment Jia, Zhaoheng; Huazhong Agricultural University, College of Resources & Environment Tan, Wenfeng; Key Laboratory of Subtropical Agriculture Resource and Environment, Ministry of Agriculture, College of Resources & Environment, Huazhong Agricultural University, Suib, Steven; University of Connecticut, U-60, Department of Chemistry Ge, Le; Argonne National Laboratory, Chemical Sciences and Engineering Division Qiu, Guohong; Huazhong Agricultural University, College of Resources & Environment Hu, Ronggui; Huazhong Agricultural University, College of Resources & Environment

Environmental Significance

Iron oxide nanominerals have excellent surface reactivity and adsorption capacity due their high specific surface area. Therefore, iron oxide nanominerals can act as sinks for inorganic cations (such as Al^{3+}, Mn^{2+}, Cu^{2+}, Zn^{2+}, Co^{2+}, Ni^{2+} and Pb^{2+}), inorganic anions (such as PO_4^{3-}, SiO_3^{2-}, MoO_4^{2-} and AsO_4^{3-}) and organic compounds (such as humic acid, citric acid, fulvic acid and antiseptic) in soils and sediments. The adsorption and redox reactivity for these nutrient elements and trace metals are affected by the formation and transformation of iron oxides. This study reveals the formation of iron oxide nanoparticles through photocatalytic oxidation of $Fe^{2+}{}_{aq}$ in the presence of nitrate. In addition, $Fe^{2+}{}_{aq}$ promotes the transformation of the photosynthetic schwertmannite to goethite and lepidocrocite by dissolution–recrystallization. Our results demonstrate the importance of photochemistry of nitrate in the formation of iron oxide nanominerals in aqueous geochemistry.

Abiotic photomineralization and transformation of iron oxide nanominerals in aqueous systems†

Lihu Liu,[a] Zhaoheng Jia,[a] Wenfeng Tan,[a] Steven L. Suib,[b] Le Ge,[c] Guohong Qiu*[a] and Ronggui Hu[a]

[a] Key Laboratory of Arable Land Conservation (Middle and Lower Reaches of Yangtse River), Ministry of Agriculture, College of Resources and Environment, Huazhong Agricultural University, Wuhan 430070, Hubei Province, China

[b] Department of Chemistry, University of Connecticut, Storrs, 55 North Eagleville Road, Storrs, Connecticut, 06269-3060, USA

[c] Chemical Sciences and Engineering Division, Argonne National Laboratory, 9700 S Cass Ave., Argonne, IL 60439, USA

* Corresponding author: Qiu GH, qiugh@mail.hzau.edu.cn

† Electronic supplementary information (ESI) available.

Abstract: The formation and transformation of iron oxide nanominerals in water environment control the migration and conversion of essential and toxic elements and organic pollutants. This study demonstrates the formation of iron oxide nanominerals through the oxidation of Fe^{2+}_{aq} by hydroxyl radicals ($OH^{\bullet}$) and superoxide radicals ($O_2^{\bullet-}$) generated from the photolysis of nitrate. The mineral compositions were affected by the anion species and pH. In the photochemical system, schwertmannite was formed in 5.0 mmol L^{-1} SO_4^{2-} solution with the initial pH of 6.0, and a mixture of goethite and lepidocrocite was formed when the SO_4^{2-} concentration decreased to 0.1 mmol L^{-1}. The particle size of schwertmannite increased with decreasing initial pH from 6.0 to 3.0. When Cl^- was used instead of SO_4^{2-}, single-phase lepidocrocite was formed with the initial pH of 6.0. When the initial pH decreased to 4.5 and 3.0, a mixture of goethite and lepidocrocite was formed, and the

relative content of lepidocrocite decreased with decreasing initial pH. Under anoxic condition, Fe^{2+}_{aq} promoted the transformation of the photochemical synthesized schwertmannite to goethite and lepidocrocite by dissolution–recrystallization. The present work expands our understanding of the generation and transformation of iron oxide nanominerals in nitrate-rich supergene environments.

1. Introduction

Iron is the most abundant transition metal in the earth crust, and their corresponding oxide minerals (including oxides, hydrates and hydrated oxides) are the most important metal oxide minerals in soils and sediments.[1,2] Iron oxide nanominerals, which have small particle size and high catalytic activities and adsorption capacities, control the distribution, transformation and bioavailability of many nutrients and pollutants including toxic organics and heavy metals, and drive the biogeochemical cycling of C, N, S and P in some redox environments.[1–6] The formation and transformation of iron oxide nanominerals have been widely studied in the fields of soil science, mineralogy, environmental science, materials science, and microbiology over the last half century.[6–10]

In natural environments, the oxidation processes of Fe^{2+}_{aq} to Fe(III) oxides are mainly mediated by microorganisms.[6,10,11] In acidic oxic environments, acidophilic Fe(II)-oxidizing bacteria can oxidize Fe^{2+}_{aq} to Fe(III) oxides using O_2; in anoxic environments, the oxidation of Fe^{2+}_{aq} by microorganisms can occur through photosynthetic Fe(II) oxidation and nitrate-dependent Fe(II) oxidation.[6,10,11] Fe^{2+}_{aq} can exist in nitrate-containing wastewaters,[12,13] and nitrate-dependent Fe(II) oxidation has been ubiquitously found in activated sludge, marine sediments and anoxic aquifer sediments.[11,14] Iron oxides including goethite, lepidocrocite, ferrihydrite and green rust can be generated from nitrate-dependent Fe(II) oxidation.[11]

The concentrations of nitrate ions have significantly increased in surface waters all over the world due to human activities, especially the excessive use of nitrogen fertilizer in agriculture and the emission of nitrogen-containing wastewaters.[15] High concentration of nitrate in surface waters results in eutrophication, and the concentrations of nitrate even exceed 0.1 mmol L^{-1} in some eutrophic waters.[16] For example, the highest concentration of nitrate reached 14.2 mg L^{-1} (0.23 mmol L^{-1}) in Taihu Lake (the third largest freshwater lake in China) during 2006 to 2008.[17] In Chaohu Lake (one of the five largest freshwater lakes in China), the highest concentration of nitrate in the surface waters reached 13.6 mg L^{-1} (0.22 mmol L^{-1}) in November of 2013.[18]

Light can penetrate the sandy sediments with a thickness of about 5–6 mm, and reach about 100 m underwater through a water column.[6] Nitrate was found to be photoreactive a few decades ago, and it can produce reactive oxygen species (ROS) including hydroxyl radicals ($OH^{\bullet}$) and superoxide radicals ($O_2^{\bullet-}$) under ultraviolet irradiation.[19,20] The two radicals are strong oxidizers in natural systems.[21] Low-valence metal ions including Fe^{2+}_{aq}, Mn^{2+}_{aq}, Tl^{+}_{aq}, Ag^{+}_{aq}, Cu^{2+}_{aq} and Sn^{2+}_{aq} can be oxidized to high-valence metal ions or oxides by ROS.[22] Hence, besides the oxidation mediated by microorganisms, the oxidation of Fe^{2+}_{aq} by nitrate photolysis may be another generation pathway of Fe(III) oxides in nitrate-rich wastewaters, eutrophic waters and sediment surface under various light conditions. However, the oxidation mechanisms of Fe^{2+}_{aq} to Fe(III) oxide minerals by the photolysis of nitrate remain elusive, and little is known about the effects of reaction conditions on the crystal structure of products formed in the photochemical processes.[3,23–25]

In addition, iron oxides formed under different conditions have different crystal structures and micromorphologies, which affect the transformation process of iron oxides.[9,11,25] There are differences in the transformation rates of goethites with different micromorphologies and surface properties to magnetite.[9] As the product of many biotic and abiotic processes, Fe^{2+}_{aq} can be adsorbed on the surface of Fe(III) oxides. Electron transfer can occur between the absorbed Fe^{2+} and Fe(III) in iron oxides, which promotes the transformation of Fe(III) oxides to other Fe(III) or Fe(II)–Fe(III) mixed-valence phases.[9,26] Hence, the transformation of iron oxides formed by photochemical oxidation may be different from that of iron oxides formed by chemical and microbial oxidation.

Schwertmannite, a nanocrystalline ferric oxyhydroxy-sulfate mineral ($Fe_8O_8(OH)_{8-2x}(SO_4)_x$, $1 < x < 1.75$), widely exists in acid mine drainage and sulfate-rich sediments, and can adsorb arsenic and other trace elements due to its large specific surface area.[27,28] Therefore, the formation and transformation of schwertmannite can strongly influence water quality in acid-sulfate systems.[27,28] Schwertmannite usually acts as the precursor for the formation of goethite and lepidocrocite. Although the transformation products of schwertmannite in the presence of Fe^{2+} have been well characterized, there is a lack of visual evidences of the transformation process by electron transfer and dissolution–recrystallization.[28,29] The study of the further transformation of the photochemical synthesized schwertmannite will facilitate the understanding of the varieties of iron oxides induced by solar irradiation in natural environments.

Here, iron oxide nanominerals including schwertmannite, lepidocrocite and goethite were generated by photocatalytic oxidation of Fe^{2+}_{aq} in the presence of nitrate under UV and solar irradiation in nitrogen atmosphere. The changes in the crystal structures and micromorphologies of the iron oxide nanominerals were investigated under different pHs and anion species. The transformation of the photochemical synthesized schwertmannite was further investigated using XRD and FESEM in the presence of Fe^{2+}_{aq}. The study was expected to facilitate a better understanding of the formation and transformation of iron oxide nanominerals in supergene environments.

2. Experimental

2.1 Photochemical formation of iron oxide nanominerals

The deoxygenated deionized water was prepared as follows. The distilled deionized water was first boiled for 15 min, and then cooled to room temperature. High-purity nitrogen gas (99.999%, Wuhan Iron and Steel (Group) Corp., China) was continuously admitted into the deionized water during the cooling process. All solutions were prepared with deoxygenated deionized water in an anaerobic glove box (YQX-II, CIMO Medical Instrument Manufacturing Co., Ltd, Shanghai, China) protected by high-purity nitrogen gas. In a typical experiment, a 100-mL mixed solution of $FeSO_4$/$FeCl_2$ (0.1–5.0 mmol L^{-1}) and $NaNO_3$ (0–100 mmol L^{-1}) was respectively prepared in a 150 mL quartz tube. The initial pH of the mixed solution of $FeSO_4$ and $NaNO_3$ was adjusted using H_2SO_4 (0.1 mol L^{-1}) and NaOH (0.1 mol L^{-1}), and that of the mixed solution of $FeCl_2$ and $NaNO_3$ was adjusted using HCl (0.1 mol L^{-1}) and NaOH (0.1 mol L^{-1}). Then, the sealed quartz tubes were taken out from the anaerobic glove box and exposed to solar irradiation for different time periods. 4-morpholinopropanesulfonic acid (MOPS) was used to control the pH in the formation and transformation of iron oxides.[28] In order to reduce the effect of pH fluctuation on the formation of iron oxide nanominerals, the pHs of the reaction systems of $FeSO_4$/$FeCl_2$ (5.0 mmol L^{-1}) and $NaNO_3$ (100 mmol L^{-1}) under solar irradiation were further controlled at 6.0 using MOPS (100 mmol L^{-1}) and NaOH (0.1 mol L^{-1}). In order to investigate the role of SO_4^{2-} on the formation of schwertmannite, additional 0.9 mmol L^{-1} Na_2SO_4 was added to the reaction system of $FeSO_4$ (0.1 mmol L^{-1}) and $NaNO_3$ (0.2 mmol L^{-1}) under UV and solar irradiation for 6 h in nitrogen atmosphere. The experiments under solar irradiation were conducted on the rooftop of College of

Resources and Environment building (E 114°21′12″, N 30°28′34″), Huazhong Agricultural University. The light intensity was 0.24–1.78 mW cm^{-2} at 320–400 nm. The precipitates were obtained using centrifugal separation and washed with distilled deionized water and dried at 40 °C overnight.

In order to investigate the formation mechanism of iron oxide minerals, the above experiments were performed under ultraviolet (UV), visible (Vis) light and dark conditions. The reactions under UV irradiation were conducted in photoreactor of PL-03 (6.61×10^3 μW cm^{-2} at 320–400 nm, Beijing Precise Technology Co., Ltd.). The experiments under Vis light were performed in photoreactor of PL-03 (4.22×10^3 μW cm^{-2} at 400–1000 nm, Beijing Precise Technology Co., Ltd.) equipped with a xenon lamp, and the UV light was removed by a filter. The prepared $FeSO_4$ solution were placed in air atmosphere under dark condition to compare the oxidation rates of Fe^{2+} by air and photolysis of nitrate.

2.2 Schwertmannite transformation

The transformation of the photochemical synthesized schwertmannite in the presence of $Fe^{2+}{}_{aq}$ was performed at a constant pH of 6.0 under anoxic conditions. The preparation of the solutions and transformation of the schwertmannite were performed in an anaerobic glove box protected by high-purity nitrogen gas at 25 °C. 200 mL $NaNO_3$ (100 mmol L^{-1}) solution was prepared, and the pH was controlled at 6.00 ± 0.05 using MOPS (50 mmol L^{-1}) and NaOH (0.1 mol L^{-1}). 0.1 g of schwertmannite was added into the $NaNO_3$ solution under stirring for 24 h. Then, 0.0556, 0.1296, 0.2591 and 0.3887 g of $FeSO_4{\cdot}7H_2O$ was respectively added into the suspensions. The corresponding concentration of $Fe^{2+}{}_{aq}$ was 1.00, 2.33, 4.66 and 6.99 mmol L^{-1}, and the corresponding molar ratio of $Fe^{2+}{}_{aq}$ to Fe(III) in schwertmannite was 0.21, 0.50, 1.00 and 1.50.

After a period of reaction time, about 10 mL solution in reaction system was drawn off and filtered by a 0.22 μm microporous membrane (Shanghai Xinya Purification Material Factory). The solid products were characterized by XRD.

2.3 Analytical methods

The as-obtained samples were characterized by power X-ray diffractometer (XRD, Bruker D8 ADVANCE) with Ni-filtered Cu Kα radiation, Fourier-transform infrared spectroscopy (FTIR, Bruker VERTEX 70), Raman spectroscopy (Renishaw inVia micro-Raman spectroscopy system, 633 nm laser), field-emission scanning electron microscopy (FESEM, Hitachi, SU8000), and high-resolution transmission electron microscopy (HRTEM, FEI, Talos F200C). The intensity of UV and Vis light was respectively determined by UV-A and FZ-A irradiatometer (Photoelectric Instrument Factor of Beijing Normal University). The UV−Vis adsorption spectra of nitrate were obtained using a spectrophotometer (Lambda 650S, Perkin-Elmer) at a scanning rate of 266.75 nm min^{-1}, and the slit width was 1 nm. The concentration of $Fe^{2+}{}_{aq}$ in solution was determined by an atomic absorption spectroscopy (Varian AA240FS). The concentration of nitrite was determined by an ion chromatography (Dionex ICS-1100).

To examine the existence of ROS in the photochemical formation of iron oxides, $OH^•$ and $O_2^{•-}$ were scavenged by 0.02 mol L^{-1} of *tert*-butyl alcohol (*t*-BuOH) and 10 mg L^{-1} of superoxide dismutase (SOD), respectively.[30] In order to quantify the $OH^•$, benzoic acid (BA) (10 mmol L^{-1}) was added to the reaction system at the initial stage. Hydroxyl radicals can participate in the oxidation of BA (10 mmol L^{-1}) to form *p*-hydroxybenzoic acid (*p*-HBA), which can be determined at 255 nm by high-performance liquid chromatography (Agilent, HPLC-1200).[31]

The chemical formulas of the synthesized schwertmannites can be written as

$Fe_8O_8(OH)_x(SO_4)_y{\cdot}zH_2O$, where $x = 8 - 2y$. About 0.1 g sample was dissolved using 50 mL hydrochloric acid (0.1 mol L^{-1}) at 50 °C to determine the chemical composition of schwertmannite. The ratio of Fe to SO_4^{2-} in schwertmannite was analyzed by atomic absorption spectroscopy (Varian AA240FS) and ion chromatography (Dionex ICS-1100). The adsorbed water in schwertmannite was calculated by mass conservation. The molar ratio of Fe/S in schwertmannite was also analyzed by X-ray photoelectron spectroscopy with Al Kα at 1486.71 eV (XPS, VG Multilb2000, Thermo Electron Corporation, USA), and charge referencing was carried out with the C 1s peak (284.6 eV).

3. Results

3.1 Formation of iron oxide nanominerals

To examine the photocatalytic effect of nitrate ions on the formation of iron oxide nanominerals, the mixed solutions of $FeSO_4/FeCl_2$ (0.1 mmol L^{-1}) and $NaNO_3$ (0.2 mmol L^{-1}) with initial pH of 6.0 were exposed to solar irradiation for 12 h in nitrogen atmosphere. The XRD patterns of solid products indicated that a mixture of goethite and lepidocrocite was formed (Fig. 1a) in the above photochemical systems of $FeSO_4/FeCl_2$. Diffraction peaks with *d* values of 0.408, 0.271, 0.239 and 0.223 nm respectively correspond to the (1 1 0), (1 3 0), (1 1 1) and (2 1 0) planes of goethite (JCPDS card No. 81-0463). Diffraction peaks with *d* values of 0.334, 0.253, 0.171 and 0.146 nm correspond to the planes of lepidocrocite (JCPDS card No. 05-0499). The corresponding TEM images of the obtained iron oxide minerals formed in the above photochemical processes indicated that goethite and lepidocrocite nanoparticles were formed (Fig. S1).

Nitrate can produce the ROS including $OH^{\bullet}$ and $O_2^{\bullet-}$ under UV irradiation.[19,20] In order to reduce the effect of light waveband on the formation of iron oxide nanominerals, these photochemical reactions were conducted under UV irradiation. The concentration of Fe^{2+}_{aq} was determined in the mixed solutions of $FeSO_4$ (0.1 mmol L^{-1}) and $NaNO_3$ (0.2 mmol L^{-1}) at different times (Fig. 1b). There was no obvious decrease in the concentration of Fe^{2+}_{aq} in nitrogen atmosphere under dark condition. In order to compare the oxidation rate of Fe^{2+}_{aq} by oxygen in air and photolysis of nitrate, the concentration of Fe^{2+}_{aq} was determined in different reaction systems. The decrease of Fe^{2+}_{aq} concentration in the reaction system without $NaNO_3$ in air atmosphere was less significant than that in the corresponding systems under UV irradiation with the addition of $NaNO_3$ in nitrogen atmosphere. These results indicated that the oxidation rate of Fe^{2+}_{aq} by air is slower than that by photolysis of nitrate.

To identify the presence of $OH^{\bullet}$ and $O_2^{\bullet-}$ radicals in the photochemical oxidation of Fe^{2+}_{aq}, *t*-BuOH and SOD were respectively added in the photochemical reaction system of $FeSO_4$ under UV irradiation (Fig. 1c). The oxidation rate of Fe^{2+}_{aq} decreased and increased when SOD and *t*-BuOH were added, respectively. When BA was added, as indicated by the concentration of generated *p*-HBA, scavenged $OH^{\bullet}$ radical concentration decreased in the $NaNO_3$ solution after the addition of $FeSO_4$ (Fig. 1d). These results indicated that $OH^{\bullet}$ and $O_2^{\bullet-}$ radicals were formed in the photochemical oxidation of Fe^{2+}_{aq}.

In order to investigate the effect of the concentrations of $FeSO_4/FeCl_2$ and $NaNO_3$ on the formation of iron oxide minerals, the mixed solutions of $FeSO_4/FeCl_2$ (5.0 mmol L^{-1}) and $NaNO_3$ (100 mmol L^{-1}) with initial pH of 6.0 were exposed to solar/UV/Vis irradiation in nitrogen atmosphere. Fig. 2 shows the photos of the products formed under solar irradiation at different times. The amounts of reddish-yellow iron oxides increased as the photochemical reaction proceeded. The XRD patterns and FESEM images of the solid products indicated that schwertmannite and lepidocrocite were respectively formed in $FeSO_4$ and $FeCl_2$ system with the initial pH of 6.0 under solar irradiation after 12 h (see Section 3.2).

Under UV irradiation, reddish-yellow iron oxides were also formed, and no solid product was generated under Vis and dark conditions (Fig. S2), which was further confirmed by the UV−Vis absorption spectra of the $NaNO_3$ solution and the mixed solution of $FeSO_4$ and $NaNO_3$ (Fig. S3). As indicated by the XRD patterns, FTIR and Raman spectra (Fig. 3a and Fig. S4a, b), schwertmannite (JCPDS card No. 47-1775) was formed in the mixed solution of $FeSO_4$ and $NaNO_3$ under UV irradiation for different time periods. Diffraction peaks at 2θ values of 18.2°, 26.3°, 35.2°, 39.5°, 46.5°, 55.3° and 61.3° were observed, which correspond to the planes of (2 1 0), (3 1 0), (2 1 2), (3 0 2), (1 1 3), (5 2 2) and (0 0 4), respectively. The TEM images of the schwertmannite formed at 48 h are shown in Fig. 3b. Needle nanocrystal clusters were aggregated together, and the lattice fringes and selected area electron diffraction patterns further confirmed the formation of schwertmannite. The chemical formula of the schwertmannite obtained after 48 h of photochemical reaction was analyzed and calculated to be $Fe_8O_8(OH)_{5.18}(SO_4)_{1.41}\cdot 5.2H_2O$, and the similar Fe/S molar ratio and chemical composition were further verified by XPS analysis (Table S1 and Fig. S5). After 48 h of photochemical reaction, the pH decreased from 6.0 to about 2.5 (Table S1). When $FeCl_2$ was used instead of $FeSO_4$ in the above photochemical systems, the XRD patterns, FTIR and Raman spectra of the solid products indicated the formation of lepidocrocite at different times (Fig. 3c and Fig. S4c, d). Fig. 3d shows the FESEM image of the lepidocrocite formed at 48 h, which indicates a typical lamellar structure. These results indicated that the as-obtained schwertmannite and lepidocrocite were not transformed into other iron oxides in the photochemical system within 48 h.

The results of reaction systems with different concentrations of $Fe^{2+}{}_{aq}$ and NO_3^- under solar irradiation indicated that iron oxide nanominerals could also be generated in the aqueous reaction systems with higher concentrations of $Fe^{2+}{}_{aq}$ and NO_3^-. High concentration of SO_4^{2-} and Cl^- facilitated the formation of schwertmannite and lepidocrocite, respectively. In addition, the crystal structure and micromorphology of iron oxide nanominerals formed under UV irradiation were similar to those of iron oxide nanominerals formed under solar irradiation.

3.2 Effect of pH

Iron oxide nanominerals could be formed with different concentrations of Fe salts and nitrate ions (Figs. 1 and 3–5). In the reaction system under solar irradiation, a small amount of solid product was formed in the reaction system with a low nitrate concentration, and the amount increased with increasing nitrate concentration (Fig. S6). In order to obtain larger amount of solid products to facilitate the sample characterization, a high concentration (100 mmol L^{-1}) of $NaNO_3$ was chosen to study the effects of pH and light source on the crystal structures and chemical compositions of Fe oxide nanominerals. In the aqueous systems of $FeSO_4$ (5.0 mmol L^{-1}) and $NaNO_3$ (100 mmol L^{-1}) with initial pH of 6.0 under solar irradiation, the XRD patterns of the solid products indicated that schwertmannite was formed after 12 h (Fig. 4a). There was no obvious change in the crystal structure of the as-obtained schwertmannite when the initial pH decreased to 4.5 and 3.0, and the final pHs of the above three mixed solutions all decreased to about 2.5. The chemical formulas of the synthesized schwertmannites were analyzed to be $Fe_8O_8(OH)_{5.94}(SO_4)_{1.03}\cdot3.14H_2O$, $Fe_8O_8(OH)_{5.88}(SO_4)_{1.06}\cdot3.62H_2O$ and $Fe_8O_8(OH)_{5.72}(SO_4)_{1.14}\cdot4.33H_2O$ when the initial pH was respectively adjusted to 6.0, 4.5 and 3.0 (Table S2). The Fe/S molar ratio in the schwertmannite decreased with decreasing initial pH (Table S2). The FTIR results further indicated the formation of schwertmannite (Fig. S7a).

Fig. 4b–d shows the FESEM images of the schwertmannites obtained at different initial pHs. Urchin-like architectures composed of nano-sized fibers were observed, indicating the typical micromorphology of schwertmannite. The size of the urchin-like architectures was about 500 nm, 800 nm and 1 μm when the initial pH was respectively adjusted to 6.0, 4.5 and 3.0, showing an increasing trend with decreasing initial pH. Urchin-like schwertmannite is also found in stream sediments.[32] These results suggested that schwertmannite similar to that formed in natural environments can be obtained from the oxidation of Fe^{2+}_{aq} by nitrate photolysis.

Fig. 5a shows the XRD patterns of the fabricated products when $FeCl_2$ was used as Fe^{2+}_{aq} source instead of $FeSO_4$ in the above photochemical processes. Single-phase lepidocrocite was generated at the initial pH of 6.0. When the initial pH decreased to 4.5 and 3.0, a mixture of goethite and lepidocrocite was formed. The diffraction peak intensity of goethite and lepidocrocite respectively increased and decreased with initial pH decreasing from 4.5 to 3.0. The FTIR results further indicated that single-phase lepidocrocite and a mixture of goethite and lepidocrocite were respectively formed at the initial pH of 6.0 and 4.5–3.0 (Fig. S7b). The final pHs decreased to 2.49, 2.50 and 2.43 when the initial pH was adjusted to 6.0, 4.5 and 3.0.

Fig. 5b–d shows the FESEM images of the corresponding iron oxides generated from the oxidation of $FeCl_2$ at different initial pHs. Uniform lepidocrocite nanosheets were obtained at the initial pH of 6.0. When the initial pH decreased to 4.5 and 3.0, sheet-like lepidocrocite attached by spherical goethite nanoparticles was observed, and the relative contents of nanosheets and nanoparticles respectively decreased and increased with decreasing initial pH. The micromorphologies of iron oxides formed via the photochemical reactions were similar to those of iron oxides found in some soils in nature.[3] The XRD and FESEM results indicated that high initial pH facilitates the formation of lepidocrocite.

In order to reduce the effect of pH fluctuation on the formation of iron oxide nanominerals, the pHs of the above two mixed solutions of $FeSO_4$/$FeCl_2$ and $NaNO_3$ were controlled at 6.0 using buffer solution, and then these reactions were conducted under solar light and dark conditions in nitrogen atmosphere. The decrease in pH was less than 0.2 after the photochemical reactions. Under dark condition, no solid product was formed (Fig. S8). The XRD and FESEM results of the solid products generated under solar irradiation indicated that a single-phase lepidocrocite was formed in the mixed solutions of $FeSO_4$/$FeCl_2$ and $NaNO_3$ at constant pH of 6.0 (Fig. S9).

3.3 Transformation of schwertmannite

No obvious change was observed in the crystal structure of schwertmannite with increasing reaction time. Therefore, the schwertmannite formed in the system of $FeSO_4$ (5.0 mmol L^{-1}) and $NaNO_3$ (100 mmol L^{-1}) under UV irradiation for 6 h was used to investigate the transformation process of the photochemical synthesized schwertmannite in the presence of Fe^{2+}_{aq}. As shown in Fig. 6a, no obvious change was observed in the crystal structure of the schwertmannite after hydration for 24 h in the solution without Fe^{2+}_{aq}. When Fe^{2+}_{aq} at an initial concentration of 6.99 mmol L^{-1} was added, goethite (JCPDS card No. 81-0463) and lepidocrocite (JCPDS card No. 03-0079) were formed. The intensity of diffraction peaks of schwertmannite decreased and that of goethite and lepidocrocite increased with increasing reaction time. Fig. 6b–e shows the FESEM images of the corresponding transformation products. There was no obvious change in the micromorphology of the schwertmannite after hydration for 24 h in the solution without Fe^{2+}_{aq}. In the presence of Fe^{2+}_{aq}, the dissolution of needle-like crystals on schwertmannite surface and the formation of rod-like and flake crystals were observed. With increasing reaction time, the size of rod-like and flake crystals increased, and hollow spherical structure consisting of rod-like crystals was formed, which has not been reported in the transformation of schwertmannite to goethite and lepidocrocite. The transformed products were further characterized by HRTEM. The interplanar spacings of 0.269, 0.258, 0.248 and 0.156 nm in rod-like crystals respectively correspond to the (1 3

0), (0 2 1), (0 4 0) and (1 5 1) planes of goethite. Hence, the flake crystals were lepidocrocite. Similar changing trends in the micromorphology of schwertmannite were observed in the systems with Fe^{2+}_{aq} concentrations of 1.00, 2.33 and 4.66 mmol L^{-1}, and the transformation rate increased with increasing Fe^{2+}_{aq} concentration (Fig. S10).

4. Discussion

4.1 Formation mechanisms of iron oxide nanominerals

The photochemical reaction of nitrate would occur if there was UV irradiation. Therefore, the crystal structures and micromorphologies of the products formed under solar irradiation were similar to those of the products formed under UV irradiation (Fig. S3). $NO_2^{•}$, $O(^3P)$ and $OH^{•}$ radicals can be formed through n→π* and π→π* electronic transition when nitrate is exposed to UV irradiation,[33,34] and the quantum yield of $OH^{•}$ radicals is significantly higher than that of $O(^3P)$.[33] With the addition of $FeSO_4$, the decrease of $OH^{•}$ radical concentration in the $NaNO_3$ solutions indicates that $OH^{•}$ radicals facilitate the oxidation of Fe^{2+}_{aq}. Superoxide radicals ($O_2^{•-}$) can be generated when nitrate or nitrite is exposed to UV irradiation in the presence of O_2.[21,30,35] In the photochemical oxidation of Mn^{2+}_{aq} in the presence of NO_3^-, $O_2^{•-}$ radicals were regarded as the main oxidant.[30] In this work, nitrite was also found in the photochemical reactions, which was formed from the photolysis of nitrate (Fig. S11).[33,34] Although the photochemical reactions were conducted under anoxic conditions, the photolysis of nitrate can lead to the formation O_2.[33] Therefore, $O_2^{•-}$ could be generated in this work. The significant decrease in the oxidation rate of Fe^{2+}_{aq} in the presence of SOD indicates that $O_2^{•-}$ radicals play an important role in the formation of iron oxide nanominerals. When *t*-BuOH was added, the elimination of $OH^{•}$ radicals by *t*-BuOH could promote the production of $O_2^{•-}$ radicals,[30] resulting in an increased oxidation rate of Fe^{2+}_{aq}. These results indicate that compared with $OH^{\bullet}$ radicals, $O_2^{\bullet-}$ radicals are mainly responsible for the formation of iron oxide nanominerals.

Although organic compounds in natural waters and sediments can scavenge the ROS, the oxidation of Fe^{2+}_{aq} to Fe(III) oxides by ROS is still present in some surface waters.[36] Reactive oxygen species produced from natural organic matter under irradiation can also oxidize Fe^{2+}_{aq} to Fe(III) ions or oxides.[37,38] Manganese(IV) oxides were observed to be generated from the oxidation of $O_2^{\bullet-}$ photoproduced by humic substances and during the asexual reproduction of ascomycete fungus.[39,40] Fe^{2+}_{aq} is more readily oxidized than Mn^{2+}_{aq} in natural environments. Hence, Fe^{2+}_{aq} may be oxidized to iron oxide nanominerals by the photolysis of nitrate in anoxic nitrate-rich wastewaters, eutrophic waters and sediment surface.

4.2 Effects of anion species and pH

The anion species and pH affect the crystal structures of iron oxides. Sulfate ions can support the tunnel structure and play a key role in the formation of schwertmannite.[28,29] When additional 0.9 mmol L^{-1} Na_2SO_4 was added to the mixed solution of 0.1 mmol L^{-1} $FeSO_4$ and 0.2 mmol L^{-1} $NaNO_3$, schwertmannite could be formed under UV and solar irradiation for 6 h in nitrogen atmosphere (Fig. S12). At the initial pH of 6.0, when the SO_4^{2-} concentration reached 5.0 mmol L^{-1}, the formation of single-phase schwertmannite was owing to the presence of high concentration of SO_4^{2-} (Figs. 3 and 4). Single-phase goethite can be formed from the oxidation of $FeSO_4$ by air.[24] However, in this work, when SO_4^{2-} concentration decreased to 0.1 mmol L^{-1}, the mixture of goethite and lepidocrocite rather than single-phase goethite was generated. The crystal structures of iron oxides are also affected by the oxidation rate of Fe^{2+}_{aq}.[24] Goethite and lepidocrocite can be synthesized through the slow and fast oxidation of Fe^{2+}_{aq} by bubbling air, respectively.[24] In the photochemical reactions, the oxidation rate of Fe^{2+}_{aq} by $O_2^{\bullet-}$ and $OH^{\bullet}$ radicals was significantly faster than that by air (Fig. 1b). Hence, the formation of the mixture of goethite and lepidocrocite can be ascribed to the presence of low concentration of SO_4^{2-} and fast oxidation rate.

Schwertmannite is commonly generated in acid mine drainage at the pH of 2.5–4.5, and the formation is affected by pH.[29,41] Under neutral and alkaline pH conditions, OH^- outcompetes Cl^- and SO_4^{2-} to bind Fe^{3+}, which is unfavorable for the formation of schwertmannite.[42] Therefore, no schwertmannite was formed in the mixed solution of $FeSO_4$ (5.0 mmol L^{-1}) and $NaNO_3$ (100 mmol L^{-1}) at constant pH of 6.0. When the pH was initially adjusted to 6.0, it decreased to about 4.5 after 30 min, facilitating the formation of schwertmannite (Fig. S13).

When $FeCl_2$ was used as Fe^{2+}_{aq} source, a mixture of goethite and lepidocrocite was formed, which is consistent with the previous results of $FeCl_2$ solution oxidized by air.[24] With increasing initial pH, the relative content of goethite and lepidocrocite respectively decreased and increased (Fig. 4b). Within the pH ranging from 3.0 to 6.0, the relative content of $[Fe(OH)^+]$ and $[Fe(OH)_2^0]$ increases with increasing pH. The oxidation rate of Fe^{2+}_{aq} increases because $[Fe(OH)^+]$ and $[Fe(OH)_2^0]$ are far more readily oxidized than Fe^{2+}.[43] The increase of the relative content of lepidocrocite at higher pH can be attributed to the increase of oxidation rate of Fe^{2+}_{aq}.[43]

4.3 Transformation of schwertmannite

As schwertmannite is a metastable mineral, the electron transfer between adsorbed Fe^{2+} and structural Fe(III) usually leads to the dissolution−recrystallization and transformation of schwertmannite under anoxic conditions.[28,44] At pH > 5.0, the transformation rate of schwertmannite to goethite and lepidocrocite in the presence of Fe^{2+}_{aq} was several orders of magnitude faster than that in the absence of Fe^{2+}_{aq}.[28] Therefore, there was no obvious change in the crystal structure and micromorphology of schwertmannite after hydration for 24 h in the solution without Fe^{2+}_{aq} (Fig. 6).

In the solution without Fe^{2+}_{aq}, urchin-like schwertmannite could be transformed to needle-like goethite after 543 days;[41] while the formed goethite showed a similar micromorphology with pristine schwertmannite in the presence of Fe^{2+}_{aq}.[45] In this work, the goethite generated from the transformation of the photochemical synthesized schwertmannite showed a hollow spherical structure consisting of rod-like crystals, whose diameter was close to that of pristine schwertmannite (Figs. 6e and Fig. S10). As reported, schwertmannite may be a mixture phase consisting of goethite and poorly crystalline iron oxides.[46] The needles of schwertmannite formed at 85 °C were composed of goethite nanocrystals.[46] The *d*-spacings of needles in schwertmannite formed in natural environment were found to match with those of goethite.[32] Hence, the transformation process of the photochemical synthesized schwertmannite may be as follows. In the structure of schwertmannite, Fe^{2+}_{aq} can be adsorbed on the surface of goethite and poorly crystalline iron oxides. Due to the relatively higher stability of rod-like goethite, the Fe^{2+}_{aq} adsorbed on the surface of goethite can transfer electrons to the poorly crystalline iron oxides, leading to the dissolution of poorly crystalline iron oxides and the growth of goethite. On the other hand, the electron transfer between poorly crystalline iron oxides and Fe^{2+}_{aq} adsorbed on their surface resulted in the dissolution of poorly crystalline iron oxides and the formation of flake lepidocrocite.

5. Conclusions

In this work, iron oxide nanominerals including schwertmannite, lepidocrocite, and goethite were directly generated by photocatalytic oxidation of Fe^{2+}_{aq} in the presence of nitrate under UV and solar irradiation. Mineral compositions are affected by the anion species and pH. Sulfate ions play a key role in the formation of schwertmannite. During the photochemical process, hydroxyl and superoxide radicals are formed and are responsible for the oxidation of Fe^{2+}_{aq}, and serve as the important driver for the cycling of Fe in redox environments. The photochemistry of nitrate affects the cycling of iron and the fate of contaminants in some natural environments, especially in nitrate-rich wastewaters, eutrophic waters and sediment surface. In the presence of Fe^{2+}_{aq}, the dissolution−recrystallization was observed by FESEM, which led to the transformation of the photochemical synthesized schwertmannite to rod-like goethite and flake lepidocrocite. These findings would enrich our knowledge about the formation and transformation of iron oxide minerals in aqueous geochemistry, and provide a new route for the formation and preparation of iron oxide nanominerals in the fields of environmental and material sciences.

Acknowledgements

The authors thank the National Natural Science Foundation of China (Grant Nos. 41571228 and 41425006), the National Key Research and Development Program of China (Grant No. 2017YFD0801000), the Fok Ying-Tong Education Foundation (No. 141024), and the Fundamental Research Funds for the Central Universities (No. 2662015JQ002) for financial support. Steven L. Suib acknowledges support of the US Department of Energy, Office of Basic Energy Sciences, Division of Chemical, Biological and Geological Sciences under grant DE-FG02-86ER13622.A000. Authors greatly acknowledge Dr. Branko Ruscic at Argonne National Laboratory and Prof. Fan Liu at Huazhong Agricultural University for technical discussions. The authors also thank Dr. Lihong Qin and Dr. Jianbo Cao at Public Laboratory of Electron Microscope of Huazhong Agricultural University for the help of SEM and TEM characterization.

Notes and references

1 N. Pinney and D. Morgan, *Geochim. Cosmochim. Acta*, 2013, **120**, 514–530.

2 M. F. Hochella Jr., S. K. Lower, P. A. Maurice, R. L. Penn, N. Sahai, D. L. Sparks and B. S. Twining, *Science*, 2008, **319**, 1631–1635.

3 U. Schwertmann and R. M. Taylor, in *Minerals in Soil Environment*, ed. J. B. Dixon, S. B. Weed, Soil Science Society of America, Madison, 2nd, 1989, vol. 1, ch. 8, pp. 379–438.

4 H. D. Pedersen, D. Postma, R. Jakobsen and O. Larsen, *Geochim. Cosmochim. Acta*, 2005, **69**, 3967–3977.

5 Y. C. Li, S. Yu, J. Strong and H. L. Wang, *J. Soils Sediments*, 2012, **12**, 683–693.

6 E. D. Melton, E. D. Swanner, S. Behrens, C. Schmidt and A. Kappler, *Nat. Rev. Microbiol.*, 2014, **12**, 797–808.

7 T. D. Sowers, J. M. Harrington, M. L. Polizzotto and O. W. Duckworth, *Geochim. Cosmochim. Acta*, 2017, **198**, 194–207.

8 S. Rahimi, R. M. Moattari, L. Rajabi, A. A. Derakhshan and M. Keyhani, *J. Ind. Eng. Chem.*, 2015, **23**, 33–43.

9 M. Usman, M. Abdelmoula, P. Faure, C. Ruby and K. Hanna, *Geoderma*, 2013, **197–198**, 9–16.

10 K. A. Weber, L. A. Achenbach and J. D. Coates, *Nat. Rev. Microbiol.*, 2006, **4**, 752–764.

11 K. O. Konhauser, A. Kappler and E. E. Roden, *Elements*, 2011, **7**, 89–93.

12 G. Samperio-Ramos, J. M. S. Casiano and M. G. Dávila, *Biogeochemistry*, 2016, **128**,19–34.

13 S. Löfgren and B. Boström, *Water Res.*, 1989, **23**,1115–1125.

14 J. M. Senko, T. A. Dewers, and L. R. Krumholz, *Appl. Environ. Microbiol.,* 2005, **71**, 7172–7177.

15 H. O. Tugaoen, S. Garcia-Segura, K. Hristovski and P. Westerhoff, *Sci. Total Environ.*, 2017,

599–600, 1524–1551.

16 D. B. Senn and H. F. Hemond, *Science*, 2002, **296**, 2373.

17 H. Xu, H. W. Paerl, B. Q. Qin, G. W. Zhu and G. Gao, *Limnol. Oceanogr.*, 2010, **55**, 420–432.

18 S. S. Xi, G. J. Liu, C. C. Zhou, L. Wu and R. Q. Liu, *Environ. Earth Sci.*, 2015, **74**, 1647–1655.

19 M. Daniels, R. V. Meyers and E. V. Belardo, *J. phys. Chem.*, 1968, **72**, 389–399.

20 P. L. Brezonik and J. Fulkerson-Brekken, *Environ. Sci. Technol.*, 1998, **32**, 3004–3010.

21 D.-H. Kim, J. Lee, J. Ryu, K. Kim and W. Choi, *Environ. Sci. Technol.*, 2014, **48**, 4030–4037.

22 G. V. Buxton, C. L. Greenstock, W. P. Helman and A. B. Ross, *J. Phys. Chem. Ref. Data*, 1988, **17**, 513–886.

23 S. J. Oh, S.-J. Kwon, J.-Y. Lee, J.-Y. Yoo and W.-Y.Choo, *Corros. Sci.*, 2002, **58**, 498–504.

24 A. Frini and M. E. Maaoui, *J. Colloid Interface Sci.*, 1997, **190**, 269–277.

25 R. M. Taylor, *Clays Clay Miner.*, 1984, **32**, 167–174.

26 Colleen M. Hansel, S. G. Benner and S. Fendorf, *Environ. Sci. Technol.*, 2005, **39**, 7147–7153.

27 X. M. Wang, C. H. Gu, X. H. Feng and M. Q. Zhu, *Environ. Sci. Technol.*, 2015, **49**, 10440–10448.

28 E. D. Burton, R. T. Bush, L. A. Sullivan and D. R. G. Mitchell, *Geochim. Cosmochim. Acta*, 2008, **72**, 4551–4564.

29 J. M. Blgham, U. Schwertmann, L. Carlson and E. Murad, *Geochim. Cosmochim. Acta*, 1990, **54**, 2743–2758.

30 H. Jung, T. S. Chadha, D. Kim, P. Biswas and Y.-S. Jun, *Chem. Commun.*, 2017, **53**, 4445–4448.

31 S. H. Joo, A. J. Feitz, D. L. Sedlak, and T. D. Waite, *Environ. Sci. Technol.*, 2005, **39**, 1263–1268.

32 R. A. French, M. A. Caraballo, B. Kim, J. D. Rimstidt, M. Murayama and M. F. Hochella, *Am. Mineral.*, 2012, **97**, 1469–1482.

33 J. Mack and J. R. Bolton, *J. Photochem. Photobiol. A*, 1999, **128**, 1–13.

34 N. K. Scharko, A. E. Berke and J. D. Raff, *Environ. Sci. Technol.*, 2014, **48**, 11991–12001.

35 D. Vione, V. Maurino, C. Minero and E. Pelizzetti, *Chemosphere*, 2001, **45**, 893–902.

36 B. M. Voelker and B. Sulzberger, *Environ. Sci. Technol.*, 1996, **30**, 1106–1114.

37 C. Jiang, S. Garg and T. D. Waite, *Environ. Sci. Technol.*, 2017, **51**, 10413–10422.

38 S. Garg, C. Jiang and T. David Waite, *Geochim. Cosmochim. Acta*, 2015, **165**, 14–34.

39 P. S. Nico, C. Anastasio and R. J. Zasoski, *Geochim. Cosmochim. Acta*, 2002, **66**, 4047–4056.

40 C. M. Hansel, C. A. Zeiner, C. M. Santelli and S. M. Webb, *Proc. Natl. Acad. Sci. USA*, 2012, **109**, 12621–12625.

41 J. M. Bigham, U. Schwertmann, S. J. Traina, R. L. Winland and M. Wolf, *Geochim. Cosmochim. Acta*, 1996, **60**, 2111–2121.

42 M. Q. Zhu, B. Legg, H. Z. Zhang, B. Gilbert, Y. Ren, J. F. Banfield and G. A. Waychunas, *Environ. Sci. Technol.*, 2012, **46**, 8140–8147.

43 B. Morgan and O. Lahav, *Chemosphere*, 2007, **68**, 2080–2084.

44 E. D. Burton, R. T. Bush, L. A. Sullivan and D. R. G. Mitchell, *Geochim. Cosmochim. Acta*, 2007, **71**, 4456–4473.

45 J. Jönsson, P. Persson, S. Sjöberg and L. Lövgren, *Appl. Geochem.*, 2005, **20**, 179–191.

46 J. G. Hockridge, F. Jones, M. Loan and W. R. Richmond, *J. Cryst. Growth*, 2009, **311**, 3876–3882.

Figure captions

Fig. 1 XRD patterns of the iron oxides formed in the mixed solutions of $FeSO_4$/$FeCl_2$ (0.1 mmol L^{-1}) and $NaNO_3$ (0.2 mmol L^{-1}) with initial pH of 6.0 under solar irradiation for 12 h in nitrogen atmosphere (a), and the concentrations of Fe^{2+} (b, c) in different reaction systems and *p*-HBA in the mixed solution of $NaNO_3$ (0.2 mmol L^{-1}) with/without $FeSO_4$ (0.1 mmol L^{-1}) (d) at the initial pH of 6.0 under UV irradiation for different time periods in nitrogen atmosphere.

Fig. 2 Photos of the aqueous reaction systems of $FeSO_4$ (a)/$FeCl_2$ (b) (5.0 mmol L^{-1}) and $NaNO_3$ (100 mmol L^{-1}) with the initial pH of 6.0 under solar irradiation for different time periods in nitrogen atmosphere.

Fig. 3 XRD patterns of schwertmannite (a) and lepidocrocite (c) formed under UV irradiation for different time periods and the corresponding HRTEM images of schwertmannite (b) and FESEM image of lepidocrocite (d) formed in the mixed solution of $FeSO_4$/$FeCl_2$ (5.0 mmol L^{-1}) and $NaNO_3$ (100 mmol L^{-1}) with the initial pH of 6.0 under UV irradiation for 48 h.

Fig. 4 XRD patterns (a) and the corresponding SEM images of schwertmannites formed in the mixed solution of $FeSO_4$ (5.0 mmol L^{-1}) and $NaNO_3$ (100 mmol L^{-1}) with initial pH of 3.0 (b), 4.5 (c) and 6.0 (d) under solar irradiation for 12 h in nitrogen atmosphere.

Fig. 5 XRD patterns (a) and the corresponding SEM images of iron oxides formed in the mixed solution of $FeCl_2$ (5.0 mmol L^{-1}) and $NaNO_3$ (100 mmol L^{-1}) with initial pH of 3.0 (b), 4.5 (c) and 6.0 (d) under solar irradiation for 12 h in nitrogen atmosphere.

Fig. 6 XRD patterns (a) and the corresponding SEM images of schwertmannite after hydration for 24 h (b) and the transformation products at initial Fe^{2+} concentration of 6.99 mmol L^{-1} for 0.5 h (c), 4 h (d) and 8 h (e), and the corresponding HRTEM images of the transformation products obtained at the initial Fe^{2+} concentration of 6.99 mmol L^{-1} for 8 h (f).

Figures

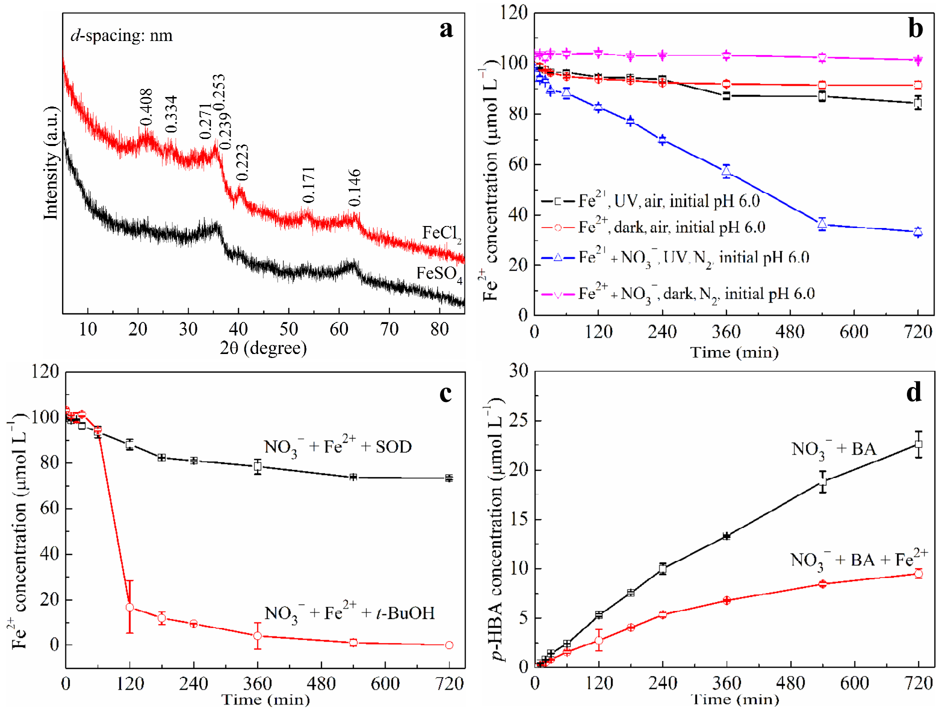

Fig. 1 XRD patterns of the iron oxides formed in the mixed solutions of $FeSO_4$/$FeCl_2$ (0.1 mmol L^{-1}) and $NaNO_3$ (0.2 mmol L^{-1}) with initial pH of 6.0 under solar irradiation for 12 h in nitrogen atmosphere (a), and the concentrations of Fe^{2+} (b, c) in different reaction systems and *p*-HBA in the mixed solution of $NaNO_3$ (0.2 mmol L^{-1}) with/without $FeSO_4$ (0.1 mmol L^{-1}) (d) at the initial pH of 6.0 under UV irradiation for different time periods in nitrogen atmosphere.

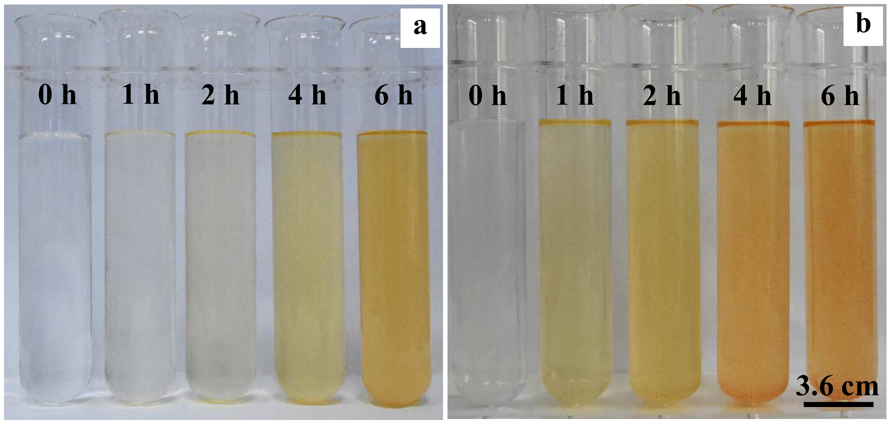

Fig. 2 Photos of the aqueous reaction systems of $FeSO_4$ (a)/$FeCl_2$ (b) (5.0 mmol L^{-1}) and $NaNO_3$ (100 mmol L^{-1}) with the initial pH of 6.0 under solar irradiation for different time periods in nitrogen atmosphere.

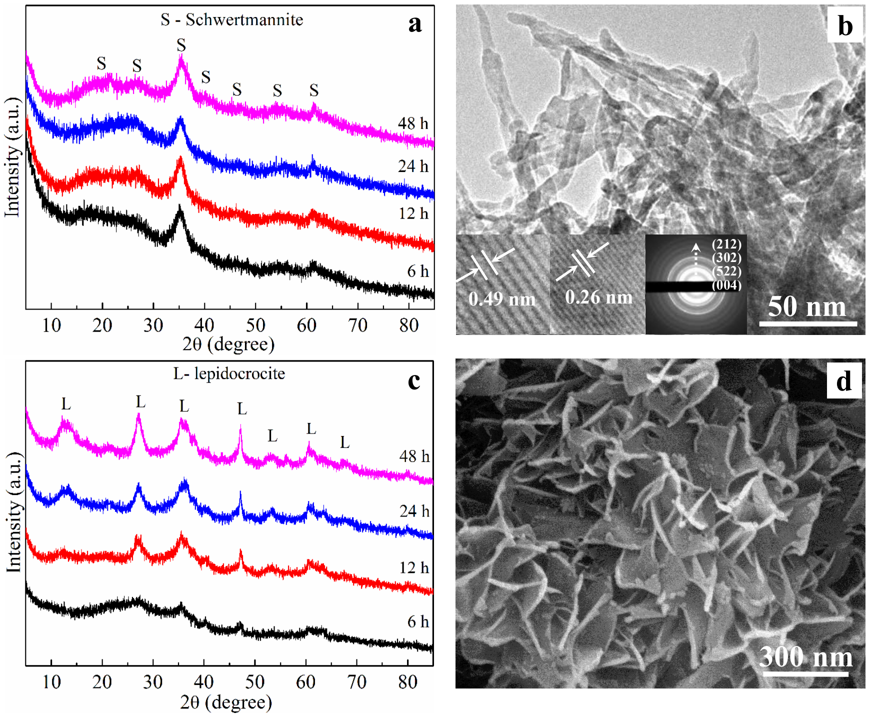

Fig. 3 XRD patterns of schwertmannite (a) and lepidocrocite (c) formed under UV irradiation for different time periods and the corresponding HRTEM images of schwertmannite (b) and FESEM image of lepidocrocite (d) formed in the mixed solution of $FeSO_4/FeCl_2$ (5.0 mmol L^{-1}) and $NaNO_3$ (100 mmol L^{-1}) with the initial pH of 6.0 under UV irradiation for 48 h.

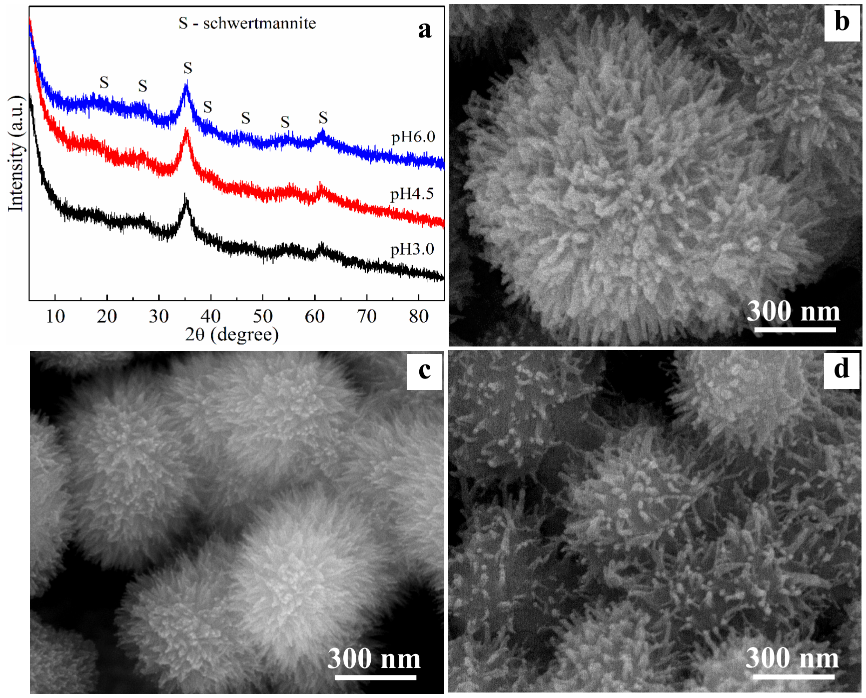

Fig. 4 XRD patterns (a) and the corresponding SEM images of schwertmannites formed in the mixed solution of $FeSO_4$ (5.0 mmol L^{-1}) and $NaNO_3$ (100 mmol L^{-1}) with initial pH of 3.0 (b), 4.5 (c) and 6.0 (d) under solar irradiation for 12 h in nitrogen atmosphere.

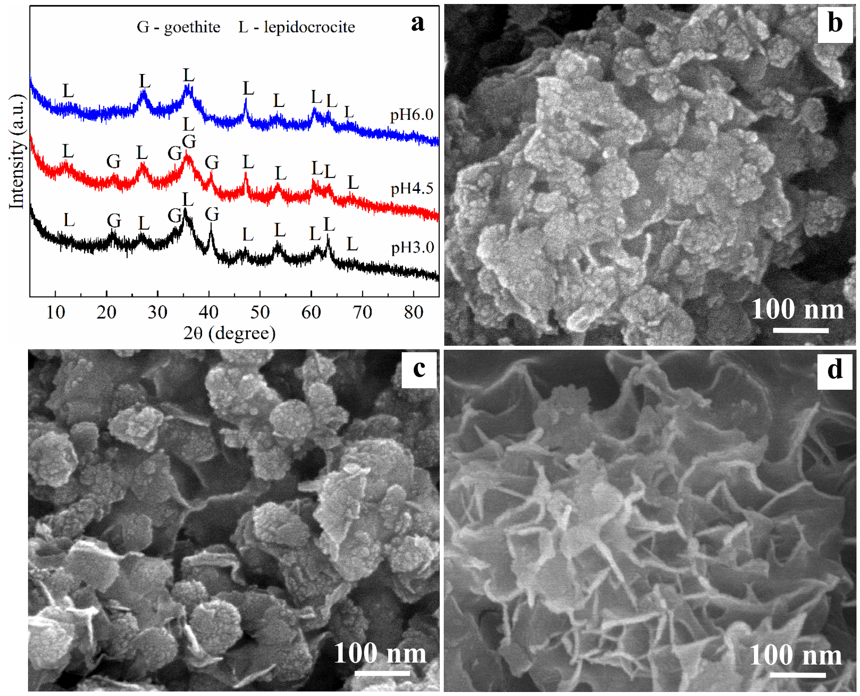

Fig. 5 XRD patterns (a) and the corresponding SEM images of iron oxides formed in the mixed solution of $FeCl_2$ (5.0 mmol L^{-1}) and $NaNO_3$ (100 mmol L^{-1}) with initial pH of 3.0 (b), 4.5 (c) and 6.0 (d) under solar irradiation for 12 h in nitrogen atmosphere.

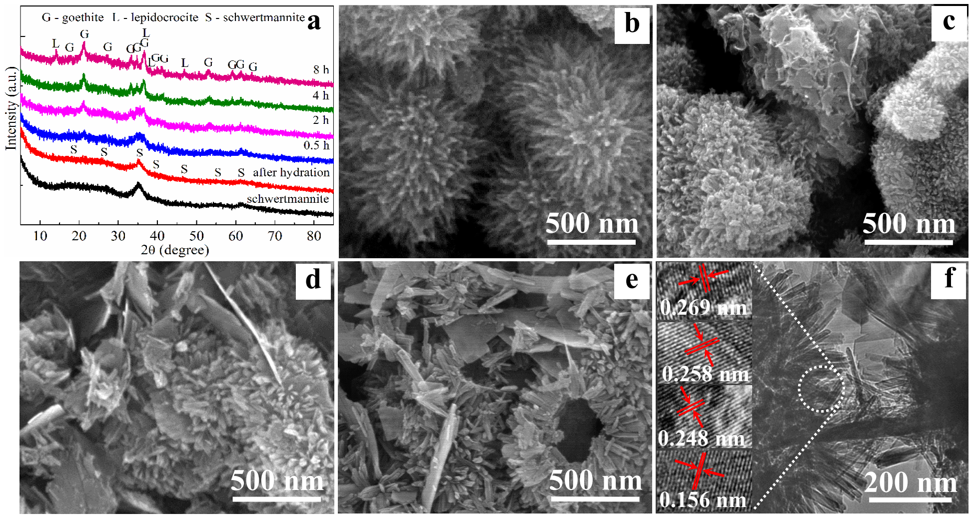

Fig. 6 XRD patterns (a) and the corresponding SEM images of schwertmannite after hydration for 24 h (b) and the transformation products at initial Fe^{2+} concentration of 6.99 mmol L^{-1} for 0.5 h (c), 4 h (d) and 8 h (e), and the corresponding HRTEM images of the transformation products obtained at the initial Fe^{2+} concentration of 6.99 mmol L^{-1} for 8 h (f).

ToC Text

Iron oxide nanominerals are generated by photocatalytic oxidation of Fe^{2+}_{aq}, and Fe^{2+}_{aq} promotes the transformation of the photochemical synthesized schwertmannite.

ToC Graphic